Chapter 7
Towards Multiple Tethered Aerial Vehicles

7.1 Modeling

In order to refer to the quantities of one component of the chain, we use the subscript $\bullet_i$ with $i = 1$ for the first link and $i = 2$ for the second. Similarly to Chap. 4 we assume: (i) negligible link masses and rotational inertias with respect to the ones of the vehicles, (ii) fixed link lengths $l_i \in \mathbb{R}_{>0}$ where $i \in \{1, 2\}$, and (iii) negligible deformations and elasticities.

We define $\varphi_i \in \mathbb{R}$ the elevation angle of the ith link. With $f_{Li} \in \mathbb{R}$ we denote the internal force that is exerted on the ith link. Also in this case the link is generic and both compressions and tensions are allowed. The first link is connected at one end to the CoM of the first vehicle, and the other end to a *fixed point*. The two ends of the second link are attached to the first and second vehicle center of masses, respectively. No rotational constraints are present in the connections, e.g., by using passive rotational joints. Finally, $m_{Ri} \in \mathbb{R}_{>0}$ and $J_{Ri} \in \mathbb{R}_{>0}$, with $i = 1, 2$, denote the mass and inertial, respectively, of the ith vehicle.

It is convenient to define the frames of the system in 3D, even if we consider a 2D problem, in order to, e.g., have a well defined angular velocity vector for the aerial vehicles. Thus we define a *world frame*, $\mathcal{F}_W$, described by the unit vector along its axes $\{\mathbf{x}_W, \mathbf{y}_W, \mathbf{z}_W\}$ and origin set on a fixed point O_W. Then, for every robot, we define a *body frame*, $\mathcal{F}_{Bi}$, rigidly attached to the ith vehicle, described by the unit vector along its axes $\{\mathbf{x}_{Bi}, \mathbf{y}_{Bi}, \mathbf{z}_{Bi}\}$ and origin O_{Bi} set on the vehicle CoM, represented in $\mathcal{F}_W$ by the coordinates $\mathbf{p}_{Bi} = \begin{bmatrix} x_{Bi} & y_{Bi} & z_{Bi} \end{bmatrix}^\top$, where $y_{Bi} = 0$. The axes $\mathbf{y}_W$, $\mathbf{y}_{B_1}$ and $\mathbf{y}_{B_2}$ are perpendicular to the vertical plane $\{\mathbf{x}_W, \mathbf{z}_W\}$ where motion occurs, as depicted in Fig. 7.1. The system evolves on this vertical plane on the effect of the four control inputs (two for each robot), i.e., the intensities $f_{Ri} \in \mathbb{R}$ and $\tau_{Ri} \in \mathbb{R}$ of the thrust force $-f_{Ri}\mathbf{z}_{Bi} \in \mathbb{R}^3$ and the torque $-\tau_{Ri}\mathbf{y}_{Bi} \in \mathbb{R}^3$, respectively, with $i = 1, 2$.

M. Tognon and A. Franchi, *Theory and Applications for Control of Aerial Robots in Physical Interaction Through Tethers*, Springer Tracts in Advanced Robotics 140,
https://doi.org/10.1007/978-3-030-48659-4_7

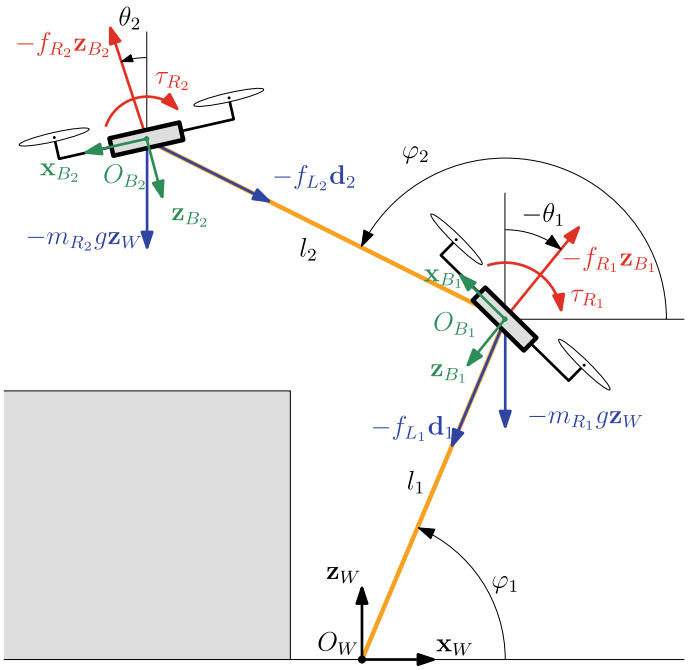

Fig. 7.1 Representation of the system and its main variables. The system is depicted in a scenario of example where the grey box represents a surface of manipulation for, e.g., a pick and place task. © 2020 IEEE. Reprinted, with permission, from [1]

Given the constraints, the system is completely described by the generalized coordinates $\mathbf{q} = [\varphi_1 \ \varphi_2 \ \theta_1 \ \theta_2]^\top = [\boldsymbol{\varphi}^\top \ \boldsymbol{\theta}^\top]^\top \in \mathbb{R}^4$, where φ_i and θ_i are the *elevation* of the ith link (defined before) and the *attitude* of the ith vehicle, respectively.

To derive the dynamic model of the system, as done in Sect. 4.3, we employ the Newton–Euler methods, because also in this case we are interest in controlling the internal force along the link and an analytical expression is thus needed. Since the rotational dynamics of the generic ith vehicle is decoupled by the translational one, we have that

$$\ddot{\boldsymbol{\theta}} = J^{-1}\tau_R, \tag{7.1}$$

where $J = \text{diag}(J_{R1}, J_{R2}) \in \mathbb{R}^{2\times 2}_{>0}$ and $\tau_R = [\tau_{R1} \ \tau_{R2}]^\top \in \mathbb{R}^2$. Since we are considering the 2D problem, in the following, we will omit the lines full of zeros relative to the $\mathbf{y}_{B_1}$ and $\mathbf{y}_{B_2}$ axes. Balancing the forces acting on the vehicle CoMs we obtain

$$\underbrace{\begin{bmatrix} m_1\ddot{\mathbf{p}}_{B_1} \\ m_2\ddot{\mathbf{p}}_{B_2} \end{bmatrix}}_{\mathbf{a}} = -\underbrace{\begin{bmatrix} \mathbf{d}_1 f_{L1} - \mathbf{d}_2 f_{L2} \\ \mathbf{d}_2 f_{L2} \end{bmatrix}}_{\mathbf{a}_{\mathbf{f}_L}} - \underbrace{\begin{bmatrix} f_{R1}\mathbf{z}_{B_1} \\ f_{R2}\mathbf{z}_{B_2} \end{bmatrix}}_{\mathbf{a}_{\mathbf{f}_R}} - \underbrace{\begin{bmatrix} m_{R1}g\mathbf{z}_W \\ m_{R2}g\mathbf{z}_W \end{bmatrix}}_{\mathbf{a}_\mathbf{g}}, \tag{7.2}$$

where $\mathbf{d}_i = [\cos\varphi_i \;\; \sin\varphi_i]^\top$ and $\mathbf{d}_i^\perp = [-\sin\varphi_i \;\; \cos\varphi_i]^\top$ are unit vectors in the vertical plane parallel and perpendicular to the ith link, respectively. The accelerations of the vehicle CoMs expressed in $\mathcal{F}_W$ are

$$\begin{aligned}\ddot{\mathbf{p}}_{B_1} &= -l_1\mathbf{d}_1\dot{\varphi}_1^2 + l_1\mathbf{d}_1^\perp\ddot{\varphi}_1\\ \ddot{\mathbf{p}}_{B_2} &= \ddot{\mathbf{p}}_{B_1} - l_2\mathbf{d}_2\dot{\varphi}_2^2 + l_2\mathbf{d}_2^\perp\ddot{\varphi}_2.\end{aligned} \tag{7.3}$$

Using (7.3) and (7.2) we have that

$$\mathbf{a} = \underbrace{\begin{bmatrix} -m_{R1}l_1\mathbf{d}_1\dot{\varphi}_1^2 \\ -m_{R2}(l_1\mathbf{d}_1\dot{\varphi}_1^2 + l_2\mathbf{d}_2\dot{\varphi}_2^2)\end{bmatrix}}_{\mathbf{a}_{\dot{\boldsymbol{\varphi}}}} + \underbrace{\begin{bmatrix} m_{R1}l_1\mathbf{d}_1^\perp & \mathbf{0} \\ m_{R2}l_1\mathbf{d}_1^\perp & m_{R2}l_2\mathbf{d}_2^\perp\end{bmatrix}}_{A_{\ddot{\boldsymbol{\varphi}}}}\ddot{\boldsymbol{\varphi}}$$

$$\mathbf{a}_{\mathbf{f}_L} = \underbrace{\begin{bmatrix}\mathbf{d}_1 & -\mathbf{d}_2 \\ \mathbf{0} & \mathbf{d}_2\end{bmatrix}}_{\mathbf{D}}\mathbf{f}_L,$$

where $\mathbf{a}_{\dot{\boldsymbol{\varphi}}} \in \mathbb{R}^4$, $\mathbf{A}_{\ddot{\boldsymbol{\varphi}}} \in \mathbb{R}^{4\times 2}$, $\mathbf{D} \in \mathbb{R}^{4\times 2}$ and $\mathbf{f}_L = [f_{L1} \;\; f_{L2}]^\top \in \mathbb{R}^2$. Therefore (7.2) can be rewritten as:

$$\underbrace{[\mathbf{A}_{\ddot{\boldsymbol{\varphi}}} \;\; \mathbf{D}]}_{\mathbf{W}}\begin{bmatrix}\ddot{\boldsymbol{\varphi}} \\ \mathbf{f}_L\end{bmatrix} = -\mathbf{a}_{\mathbf{f}_R} - \mathbf{a}_{\mathbf{g}} - \mathbf{a}_{\dot{\boldsymbol{\varphi}}}. \tag{7.4}$$

The matrix $\mathbf{W} \in \mathbb{R}^{4\times 4}$, that can be explicitly written as

$$\mathbf{W} = \begin{bmatrix} -l_1 m_{R1}\sin\varphi_1 & 0 & \cos\varphi_1 & -\cos\varphi_2 \\ l_1 m_{R1}\cos\varphi_1 & 0 & \sin\varphi_1 & -\sin\varphi_2 \\ -l_1 m_{R2}\sin\varphi_1 & -l_2 m_{R2}\sin\varphi_2 & 0 & \cos\varphi_2 \\ l_1 m_{R2}\cos\varphi_1 & l_2 m_{R2}\cos\varphi_2 & 0 & \sin\varphi_2 \end{bmatrix},$$

is full rank, in fact its determinant is $\det(\mathbf{W}) = -l_1 l_2 m_{R2}[m_{R1} + m_{R2}(1 - \cos^2(\varphi_1 - \varphi_2))]$, which is always nonzero.

The dynamics of the system is then described by the following equations:

$$\ddot{\boldsymbol{\varphi}} = \begin{bmatrix}\mathbf{I}_2 & \mathbf{0}\end{bmatrix}\boldsymbol{W}^{-1}(-\mathbf{a}_{\mathbf{f}_R} - \mathbf{a}_{\mathbf{g}} - \mathbf{a}_{\dot{\boldsymbol{\varphi}}}). \tag{7.5a}$$

$$\ddot{\boldsymbol{\theta}} = J^{-1}\tau_R \tag{7.5b}$$

For the design of a state observer in Sect. 7.4 it is useful to rewrite (7.5) in a Lagrangian format:

$$\boldsymbol{M}(\boldsymbol{\varphi})\ddot{\boldsymbol{\varphi}} = -\boldsymbol{c}(\boldsymbol{\varphi}, \dot{\boldsymbol{\varphi}}) + \bar{\mathbf{Q}}_{\boldsymbol{\varphi}}(\boldsymbol{\varphi}, \boldsymbol{\theta})\mathbf{f}_R \tag{7.6a}$$

$$J\ddot{\boldsymbol{\theta}} = \tau_R, \tag{7.6b}$$

where $\mathbf{f}_R = [f_{R1} \;\; f_{R2}]^\top$ and

$$\boldsymbol{M}(\boldsymbol{\varphi}) = \begin{bmatrix} (m_{R1} + m_{R2})l_1^2 & m_{R2}l_1l_2\cos(\varphi_1 - \varphi_2) \\ m_{R2}l_1l_2\cos(\varphi_1 - \varphi_2) & m_{R2}l_2^2 \end{bmatrix}$$

$$\boldsymbol{c}(\boldsymbol{\varphi}, \dot{\boldsymbol{\varphi}}) = \begin{bmatrix} m_{R2}l_1l_2\sin(\varphi_1 - \varphi_2)\,\dot{\varphi}_2^2 + (m_{R1} + m_{R2})gl_1\cos\varphi_1 \\ -m_{R2}l_1l_2\sin(\varphi_1 - \varphi_2)\,\dot{\varphi}_1^2 + m_{R2}gl_2\cos\varphi_2 \end{bmatrix}$$

$$\bar{\mathbf{Q}}_{\boldsymbol{\varphi}}(\boldsymbol{\varphi}, \boldsymbol{\theta}) = \begin{bmatrix} l_1\cos(\varphi_1 + \theta_1) & l_1\cos(\varphi_1 + \theta_2) \\ 0 & l_2\cos(\varphi_2 + \theta_2) \end{bmatrix}$$

7.2 Differential Flatness

For the single tethered aerial vehicle we showed that it is differentially flat with respect to $\mathbf{y}^a$ containing the position of the vehicle and the internal force along the link. In this section we shall show that analogously, the multi-robot extension here considered is differentially flat with respect to the output $\mathbf{y}_2^a = [{\mathbf{y}_{21}^a}^\top \;\; {\mathbf{y}_{22}^a}^\top]^\top = [\boldsymbol{\varphi}^\top \;\; \mathbf{f}_L^\top]^\top$, containing the position of the vehicles (parametrized by the elevation angles) and the internal force along the links.

We recall that to prove the differential flatness of the system, state, $\mathbf{x} = [x_1 \;\; x_2 \;\; x_3 \;\; x_4 \;\; x_5 \;\; x_6 \;\; x_7 \;\; x_8]^\top = [\varphi_1 \;\; \dot{\varphi}_1 \;\; \varphi_2 \;\; \dot{\varphi}_2 \;\; \theta_1 \;\; \dot{\theta}_1 \;\; \theta_2 \;\; \dot{\theta}_2]^\top \in \mathbb{R}^8$ and input, $\mathbf{u} = [f_{R1} \;\; f_{R2} \;\; \tau_{R1} \;\; \tau_{R2}]^\top = [{\mathbf{f}_R}^\top \;\; {\tau_R}^\top]^\top = [\mathbf{u}_1^\top \;\; \mathbf{u}_2^\top]^\top \in \mathbb{R}^4$, have to be expressed as an algebraic function of the output and its derivatives. We have that $\boldsymbol{\varphi}$ is already part of the output, thus $\boldsymbol{\varphi} = \mathbf{y}_{21}^a$ and $\dot{\boldsymbol{\varphi}} = \dot{\mathbf{y}}_{21}^a$. To find the rest we firstly compute the nominal thrust vectors from the output and its derivatives using (7.2):

$$\begin{bmatrix} f_{R1}\mathbf{z}_{B_1} \\ f_{R2}\mathbf{z}_{B_2} \end{bmatrix} = \mathbf{a}(\mathbf{y}_{21}^a, \dot{\mathbf{y}}_{21}^a, \ddot{\mathbf{y}}_{21}^a) + \mathbf{a}_{\mathbf{f}_L}(\mathbf{y}_2^a) + \mathbf{a}_{\mathbf{g}}. \tag{7.7}$$

Similarly to Sect. 4.4.1, from the thrust vectors we can easily compute the inputs and the missing part of the state as function of the output and its derivatives up to the fourth derivative.

Proposition *The model (7.5), is differentially flat with respect to the flat output* $\mathbf{y}_2^a = [\boldsymbol{\varphi}^\top \;\; \mathbf{f}_L^\top]^\top$. *In other words, the state and the inputs can be written as algebraic function of* $\mathbf{y}_2^a$ *and a finite number of its derivatives.* □

7.3 Dynamic Feedback Linearization

As usual, to compute the feedback linearizing control law, we need to differentiate the outputs until the input $\mathbf{u}$ appears. Inverting (7.4), and recalling that $\mathbf{y}_{21}^{a\ (2)} = \ddot{\boldsymbol{\varphi}}$ and $\mathbf{y}_{22}^{a} = \mathbf{f}_L$, we directly obtain

$$\begin{bmatrix} \mathbf{y}_{21}^{a\ (2)} \\ \mathbf{y}_{22}^{a} \end{bmatrix} = \underbrace{W^{-1}(-\mathbf{a}_{\mathbf{g}} - \mathbf{a}_{\ddot{\boldsymbol{\varphi}}})}_{\mathbf{b}(\mathbf{x})} + \underbrace{\left(-W^{-1}\begin{bmatrix}\mathbf{Z}_R & \mathbf{0}\end{bmatrix}\right)}_{\mathbf{E}(\mathbf{x})}\mathbf{u}, \tag{7.8}$$

where $\mathbf{b}(\mathbf{x})$ gathers all the terms that do not depend on $\mathbf{u}$ and $\mathbf{Z}_R \in \mathbb{R}^{4\times 2}$ is:

$$\mathbf{a}_{\mathbf{f}_R} = \begin{bmatrix} \mathbf{z}_{B_1} & \mathbf{0} & \mathbf{0}\ \mathbf{0} \\ \mathbf{0} & \mathbf{z}_{B_2} & \mathbf{0}\ \mathbf{0} \end{bmatrix}\mathbf{u} = \begin{bmatrix}\mathbf{Z}_R & \mathbf{0}\end{bmatrix}\mathbf{u}. \tag{7.9}$$

From (7.8) we can see that the input appears directly in $\mathbf{y}_{22}^{a}$ without need for differentiation while $\mathbf{y}_{21}^{a}$ has to be differentiated twice. Furthermore, we can immediately notice that the decoupling matrix $\mathbf{E}(\mathbf{x})$ is always singular which means that it is not possible to determine a static feedback that linearizes the system using $\mathbf{y}_2^a$.

As we saw in Sect. 4.6, the common technique is to delay the appearance of the input in $\mathbf{y}_{22}^{a}$ (i.e., increasing the relative degree of $\mathbf{y}_{22}^{a}$) introducing a dynamic compensator composed by one or more integrators in the input channel $\mathbf{u}_1$. To this aim, we redefine the input as $\bar{\mathbf{u}} = [\ddot{\mathbf{u}}_1^\top \ \mathbf{u}_2^\top]^\top = [\bar{\mathbf{u}}_1^\top \ \bar{\mathbf{u}}_2^\top]^\top$, considering the acceleration of the thrust intensity as new controllable input, $\ddot{\mathbf{u}}_1 = \ddot{\mathbf{f}}_R$. The system is now described by the extended state $\bar{\mathbf{x}} = \begin{bmatrix}\boldsymbol{\varphi}^\top & \dot{\boldsymbol{\varphi}}^\top & \boldsymbol{\theta}^\top & \dot{\boldsymbol{\theta}}^\top & \mathbf{u}_1^\top & \dot{\mathbf{u}}_1^\top\end{bmatrix}^\top \in \mathbb{R}^{12}$, that contains also the thrusts and their derivatives. Considering the extended system and the new input, $\mathbf{y}_{21}^{a}$ and $\mathbf{y}_{22}^{a}$ have to be differentiated four and two times, respectively, in order to see the new input $\bar{\mathbf{u}}$ appear:

$$\begin{aligned}\begin{bmatrix} \mathbf{y}_{21}^{a\ (4)} \\ \mathbf{y}_{22}^{a\ (2)} \end{bmatrix} = {} & (\ddot{W^{-1}})(-\mathbf{a}_{\mathbf{f}_R} - \mathbf{a}_{\mathbf{g}} - \mathbf{a}_{\ddot{\boldsymbol{\varphi}}}) + 2(\dot{W^{-1}})(-\dot{\mathbf{a}}_{\mathbf{f}_R} - \dot{\mathbf{a}}_{\ddot{\boldsymbol{\varphi}}}) + \\ & + (W^{-1})(-\ddot{\mathbf{a}}_{\mathbf{f}_R} - \ddot{\mathbf{a}}_{\ddot{\boldsymbol{\varphi}}}).\end{aligned} \tag{7.10}$$

In the previous equation the inputs appear only in the term $\ddot{\mathbf{a}}_{\mathbf{f}_R}$ that can be rewritten as:

$$\ddot{\mathbf{a}}_{\mathbf{f}_R} = \ddot{\mathbf{a}}'_{\mathbf{f}_R}(\bar{\mathbf{x}}) + \ddot{\mathbf{A}}''_{\mathbf{f}_R}(\bar{\mathbf{x}})\bar{\mathbf{u}}, \tag{7.11}$$

where

$$\ddot{\mathbf{A}}''_{\mathbf{f}_R}(\bar{\mathbf{x}}) = \begin{bmatrix} -\sin\theta_1 & 0 & -\frac{f_{R1}\cos\theta_1}{J_{R1}} & 0 \\ \cos\theta_1 & 0 & -\frac{f_{R1}\sin\theta_1}{J_{R1}} & 0 \\ 0 & -\sin\theta_2 & 0 & -\frac{f_{R2}\cos\theta_2}{J_{R2}} \\ 0 & \cos\theta_2 & 0 & -\frac{f_{R2}\sin\theta_2}{J_{R2}} \end{bmatrix}. \tag{7.12}$$

We can compactly rewrite (7.10) as:

$$\begin{bmatrix} \mathbf{y}_{21}^{a\,(4)} \\ \mathbf{y}_{22}^{a\,(2)} \end{bmatrix} = \mathbf{b}(\bar{\mathbf{x}}) + \underbrace{\left(-\boldsymbol{W}^{-1}\ddot{\mathbf{A}}''_{\mathbf{f}_R}(\bar{\mathbf{x}})\right)}_{\bar{\mathbf{E}}(\bar{\mathbf{x}})} \bar{\mathbf{u}}, \tag{7.13}$$

where $\mathbf{b}(\bar{\mathbf{x}})$, whose expression is omitted here for the sake of brevity, collects all the terms in (7.10) that do not depend on the input. After some algebra, it is possible to analytically compute the determinant of the new decoupling matrix $\bar{\mathbf{E}}(\bar{\mathbf{x}})$:

$$\det\left(\bar{\mathbf{E}}(\bar{\mathbf{x}})\right) = -\frac{f_{R1}f_{R2}}{J_{R1}J_{R2}l_1l_2m_{R2}\left(m_{R1}+m_{R2}\sin^2(\varphi_1-\varphi_2)\right)},$$

which is zero iff $f_{R1} = 0$ or $f_{R2} = 0$ (same singularity of the single tether case). Therefore $\bar{\mathbf{E}}(\bar{\mathbf{x}})$ is always invertible except for the cases in which one of the two thrusts vanishes. Furthermore the total relative degree $r = 8 + 4 = 12$ is equal to the dimension of the extended state $\bar{\mathbf{x}}$. This means that the system does not have an internal dynamics, i.e., it is fully linearizable through dynamic feedback. In fact, designing the control input as

$$\bar{\mathbf{u}} = \bar{\mathbf{E}}^{-1}(\bar{\mathbf{x}})\left[-\mathbf{b}(\bar{\mathbf{x}}) + \mathbf{v}\right], \tag{7.14}$$

where $\mathbf{v} = [\mathbf{v}_1^\top \ \mathbf{v}_2^\top]^\top \in \mathbb{R}^4$ is a virtual input, we obtain

$$\mathbf{y}_{21}^{a\,(4)} = \mathbf{v}_1 \qquad \mathbf{y}_{22}^{a\,(2)} = \mathbf{v}_2,$$

i.e., through the state feedback transformation (7.14) we transform the original non linear system (7.5) in a fully-equivalent linear and decoupled dynamical system.

Proposition *Consider the system composed by two aerial vehicles connected in series to the ground by two links with passive joints, whose dynamic model is described by (7.5). Consider as outputs the elevation and the internal force of the two links,* $\mathbf{y}_2^a = [\boldsymbol{\varphi}^\top \ \mathbf{f}_L^\top]^\top$. *Then the system is fully linearizable via dynamic feedback for every state configuration, iff both thrusts* f_{R1} *and* f_{R2} *are nonzero.* □

As a consequence of the previous Proposition 8, as done in Sect. 4.6 we can design a standard linear controller to obtain the tracking of a desired trajectory. The overall controller design is depicted in Fig. 7.2.

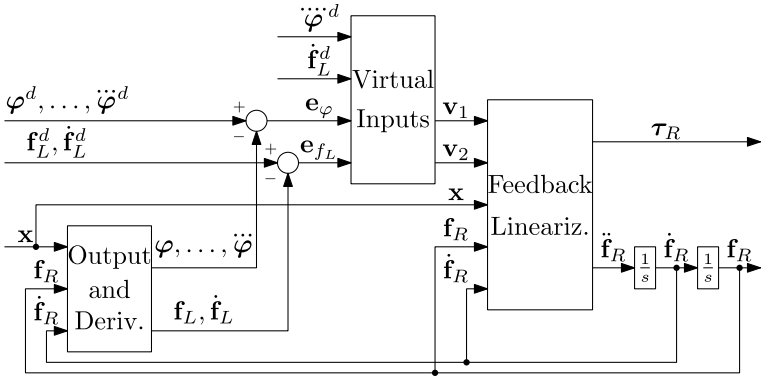

Fig. 7.2 Graphic representation of the controller. © 2020 IEEE. Reprinted, with permission, from [2]

Corollary *Let be given any desired trajectory* $\mathbf{y}_{21}^{a\,d}(t)$ *of class* C^3 *for the two links elevation* $\mathbf{y}_{21}^a$*, and any desired trajectory* $\mathbf{y}_{22}^{a\,d}(t)$ *of class* C^1 *for the two links internal force* $\mathbf{y}_{22}^a$*. Consider as input the second derivative of the two thrusts and the torques provided by the aerial vehicles,* $\bar{\mathbf{u}} = [\ddot{\mathbf{f}}_R^\top \ \tau_R{}^\top]^\top$*. Consider the control law described by (7.14) and set the virtual inputs as:*

$$\begin{aligned} \mathbf{v}_1 &= \mathbf{y}_{21}^{a\,d(4)} + \mathbf{K}_{11}\boldsymbol{e}_1 + \mathbf{K}_{12}\boldsymbol{e}_1^{(1)} + \mathbf{K}_{13}\boldsymbol{e}_1^{(2)} + \mathbf{K}_{14}\boldsymbol{e}_1^{(3)} \\ \mathbf{v}_2 &= \mathbf{y}_{22}^{a\,d(2)} + \mathbf{K}_{21}\boldsymbol{e}_2 + \mathbf{K}_{22}\boldsymbol{e}_2^{(1)}, \end{aligned} \tag{7.15}$$

where $\mathbf{K}_{ij} \in \mathbb{R}^{2\times 2}_{>0}$*, with* $i = 1 \ldots 4$ *and* $j = 1, 2$*, are diagonal matrices.*

That control law exponentially steers $\mathbf{y}_2^a$ *along any desired trajectory* $\mathbf{y}_2^{ad} = [\varphi_1^d \ \varphi_2^d \ f_{L1}^d \ f_{L2}^d]^\top$*. The behavior of the convergence can be arbitrarily assigned by suitably choosing the gain matrixes.* □

Let us define the errors as $\boldsymbol{e}_1 = \mathbf{y}_{21}^{a\,d} - \mathbf{y}_{21}^a$ and $\boldsymbol{e}_2 = \mathbf{y}_{22}^{a\,d} - \mathbf{y}_{22}^a$. The controller yields to the following error dynamics:

$$\begin{aligned} \boldsymbol{e}_1^{(4)} + \mathbf{K}_{11}\boldsymbol{e}_1 + \mathbf{K}_{12}\boldsymbol{e}_1^{(1)} + \mathbf{K}_{13}\boldsymbol{e}_1^{(2)} + \mathbf{K}_{14}\boldsymbol{e}_1^{(3)} &= 0 \\ \boldsymbol{e}_2^{(2)} + \mathbf{K}_{21}\boldsymbol{e}_2 + \mathbf{K}_{22}\boldsymbol{e}_2^{(1)} &= 0. \end{aligned}$$

Therefore, from basic linear system theory, one can arbitrarily assign the poles of the dynamics of the error in order to guaranties an arbitrarily fast exponential tracking of $(\mathbf{y}_{21}^{a\,d}(t), \mathbf{y}_{22}^{a\,d}(t))$ for $(\mathbf{y}_{21}^a(t), \mathbf{y}_{22}^a(t))$ by suitably choosing the gains: $\bar{\mathbf{K}}_1 = [\mathbf{K}_{11} \ \mathbf{K}_{12} \ \mathbf{K}_{13} \ \mathbf{K}_{14}] \in \mathbb{R}^{2\times 8}_{>0}$ and $\bar{\mathbf{K}}_2 = [\mathbf{K}_{21} \ \mathbf{K}_{22}] \in \mathbb{R}^{2\times 4}_{>0}$. Since $(\mathbf{y}_{21}^{a\,d(4)}(t), \mathbf{y}_{22}^{a\,d(2)}(t))$ have to be well defined, the elevation and internal force trajectories have to be of class C^3 and C^1 respectively.

Due to Proposition 8, if the links are bars, it is feasible to pass from compression to tension and viceversa. Instead, in the case of a cable, it is possible to maintain a

sufficient value of tension under a maximum breaking value and above the minimum tautness value.

We remark that, since the total relative degree is equal to the dimension of the extended state, there is no internal dynamics. This implies that the dynamics of the pitch of each vehicles is stable during the tracking of the desired output.

Remark (*Case of zero thrust*) If a particular desired trajectory of the outputs requires zero thrust on one of the two vehicles the controller cannot be applied, indeed in this case it has a singularity. Thus, this fact has to be considered in the planning phase in order to design desired trajectories that ensure strictly positive, or negative, thrusts. Although this is a planning problem that does not concern this work, we believe that the problem of zero thrust does not imply a strong limitation on the set of the feasible trajectories. Indeed, as it is shown in Sect. 7.5, we can still generate non-trivial trajectories, e.g., inversion of the internal link force from tension to compression, ensuring non zero thrusts. An extended study on the planning of feasible trajectories is left as future work. □

Looking at the control law described by the Eqs. (7.14) and (7.15), and depicted in the block diagram of Fig. 7.2, one can notice that its implementation requires the knowledge of the extended state $\bar{\mathbf{x}}$, the output $\mathbf{y}$ and its derivatives (up to the third-order for $\mathbf{y}_{21}^a$ and first-order for $\mathbf{y}_{22}^a$). Nevertheless, $\mathbf{y}$ and all its needed derivatives can be calculated as function of $\mathbf{x}$ and $\bar{\mathbf{u}}$ as done, e.g., in (7.8) and (7.13) for some of the derivatives. Note also that $\mathbf{u}_1$ and $\dot{\mathbf{u}}_1$ are directly known because they are internal state of the controller.

7.4 State Estimation

Instead of considering a direct measure of the state to close the control loop, we aim to find the minimal set of sensors based on which we can obtain an estimation of the state. Inspired by the results obtained in Chap. 4 we consider the possible sensory setup of Table 7.1. In this section, for the case 4 of Table 7.1, we present a method to transform the original measurements into direct measurements of the configuration $\mathbf{q}$ and we show that this implies the observability of the full state, i.e., $\mathbf{q}$ and $\dot{\mathbf{q}}$. For this case we propose a nonlinear estimator, based on the HGO able to retrieve the state from any dynamic condition. In the end we analyze the applicability of the method to the other configurations of Table 7.1.

7.4.1 Output Transformations

Assume to have an onboard accelerometer for each robot, placed at O_{B_i} and attached to $\mathcal{F}_{Bi}$. According to the model in Sect. 3.4, it measures the specific acceleration:

Table 7.1 Possible sensors configurations. The $1st$ sensor type corresponds to an accelerometer mounted on each robot

Case	$2nd$ Sensor type	Mounting place	Measures ρ_1, ρ_2	Applicability
1	Absolute Inclinom.	$\mathcal{F}_{B1}$	θ_1	Yes
	Absolute Inclinom.	$\mathcal{F}_{B2}$	θ_2	
2	Absolute Inclinom.	$\mathcal{F}_{B1}$	θ_1	Yes
	Relative Inclinom.	$\mathcal{F}_{B2}$	$\theta_1 - \theta_2$	
3	Encoder	$\mathcal{F}_W - link_1$	φ_1	No
	Encoder	$\mathcal{F}_{B1} - link_1$	$\varphi_1 + \theta_1$	
4	Encoder	$\mathcal{F}_W - link_1$	φ_1	Yes
	Encoder	$\mathcal{F}_{B1} - link_2$	$\varphi_2 + \theta_1$	
5	Encoder	$\mathcal{F}_W - link_1$	φ_1	No
	Encoder	$\mathcal{F}_{B2} - link_2$	$\varphi_2 + \theta_2$	
6	Encoder	$\mathcal{F}_{B1} - link_1$	$\varphi_1 + \theta_1$	No
	Encoder	$\mathcal{F}_{B1} - link_2$	$\varphi_2 + \theta_1$	
7	Encoder	$\mathcal{F}_{B1} - link_1$	$\varphi_1 + \theta_1$	No
	Encoder	$\mathcal{F}_{B2} - link_2$	$\varphi_2 + \theta_2$	

$$\mathbf{a}_i = R_W^{B_i}(\ddot{\mathbf{p}}_{B_i} + g z_W) = \begin{bmatrix} a_{i_x} & 0 & a_{i_z} \end{bmatrix}^\top, \tag{7.16}$$

where $R_W^{B_i} \in \mathbb{R}^3$ is the rotation matrix from $\mathcal{F}_W$ to $\mathcal{F}_{Bi}$, and $\ddot{\mathbf{p}}_{B_i}$ is the acceleration of the CoM of the ith vehicle w.r.t. $\mathcal{F}_W$.

Then we assume to be in the case #4 of Table 7.1, i.e., the system is equipped with two encoders, one is rigidly attached to the ground and connected to the first link and measures its absolute elevation relative to $\mathcal{F}_W$, while the second is fixed to $\mathcal{F}_{B1}$ and connected to the second link, and measures its relative elevation with respect to $\mathcal{F}_{B1}$, i.e.:

$$\rho_1 = \varphi_1, \qquad \rho_2 = \varphi_2 + \theta_1. \tag{7.17}$$

Now, replacing $\ddot{\mathbf{p}}_{B_2}$ from (7.2) into (7.16) for $i = 2$, we obtain

$$-m_{R2}\mathbf{a}_2 = R_W^{B_i}(f_{L2}\mathbf{d}_2 + f_{R2}z_{B_2}) = f_{L2}R_W^{B_i}\mathbf{d}_2 + [0\ 0\ f_{R2}]^\top, \tag{7.18}$$

which allows to define the measurement transformation

$$\begin{bmatrix} w_1(k) \\ w_2(k) \end{bmatrix} = \begin{bmatrix} \operatorname{sgn}\left(k - \frac{1}{2}\right)\sqrt{\bar{a}_{2_x}^2 + \bar{a}_{2_z}^2} \\ \operatorname{atan2}\left(\frac{\bar{a}_{2_z}}{w_1(k)}, \frac{\bar{a}_{2_x}}{w_1(k)}\right) \end{bmatrix} = \begin{bmatrix} 0 \\ \varphi_2 + \theta_2 + \frac{\pi}{2} \end{bmatrix} \pm \begin{bmatrix} f_{L2} \\ \frac{\pi}{2} \end{bmatrix}, \tag{7.19}$$

where $\bar{a}_{2_x} = m_{R2} a_{2_x}$, $\bar{a}_{2_z} = m_{R2} a_{2_z} + f_{R2}$ and $k \in \{0, 1\}$. Note that *[(i)]* there are two solutions for $k = 0$ and $k = 1$ because $\text{sgn}\left(f_{L2}\right)$ is not retrievable from the measurements; *[(ii)]*the transformation is allowed iff $f_{L2} \neq 0$.

At every time instant t there is only one *correct* pair of measurements, equal to $(f_{L2},\ \varphi_2 + \theta_2)$, while the other is *wrong* and equal to $(-f_{L2},\ \varphi_2 + \theta_2 + \pi)$. We define k^* the unique $k \in \{0, 1\}$ such that $(w_1(k^*),\ w_2(k^*)) = (f_{L2},\ \varphi_2 + \theta_2)$. Then, replacing $\ddot{\mathbf{p}}_{B_1}$ from (7.2) into (7.16) for $i = 1$, and after some simple algebra, we can define two additional new measurement transformations:

$$\begin{bmatrix} w_3(k^*, j) \\ w_4(k^*, j) \end{bmatrix} = \begin{bmatrix} \text{sgn}\left(j - \frac{1}{2}\right)\sqrt{\bar{a}_{1_x}^2 + \bar{a}_{1_z}^2} \\ \text{atan2}\left(\dfrac{\bar{a}_{1_z}}{w_3(k^*, j)},\ \dfrac{\bar{a}_{1_x}}{w_3(k^*, j)}\right) \end{bmatrix} = \begin{bmatrix} 0 \\ \varphi_1 + \theta_1 + \frac{\pi}{2} \end{bmatrix} \pm \begin{bmatrix} f_{L1} \\ -\frac{\pi}{2} \end{bmatrix}, \tag{7.20}$$

where $\bar{a}_{1_x} = m_{R1} a_{1_x} - w_1(k^*) \cos \rho_2$, $\bar{a}_{1_z} = m_{R2} a_{1_z} - w_1(k^*) \sin \rho_2 + f_{R2}$ and $j \in \{0, 1\}$. As in (7.19), the transformation is not possible when $f_{L1} = 0$. A practical solution for the instantaneous zero internal force case is provided in Sect. 7.4.5.

Since the sign of f_{L1} is not retrievable from the measurements, we obtain two solutions parametrized by j, i.e., $(w_3(k^*, j),\ w_4(k^*, j))$. At every time instant t there is only one *correct* pair of measurements equal to $(f_{L1}, \varphi_1 + \theta_1)$, while the other is *wrong* and equal to $(-f_{L1}, \varphi_1 + \theta_1 + \pi)$. Actually, recalling that also $k \in \{0, 1\}$, we obtain four groups of different measurements, i.e., $(w_1(k),\ w_2(k),\ w_3(k, j),\ w_4(k, j))$ with $k, j \in \{0, 1\}$. We know that at each time t there is only one couple $k^*, j^* \in \{0, 1\}$ such that the corresponding measurements are *correct*, i.e., $(w_1(k^*),\ w_2(k^*),\ w_3(k^*, j^*),\ w_4(k^*, j^*)) = (f_{L2}, \varphi_2 + \theta_2, f_{L1}, \varphi_1 + \theta_1)$, while all the others are *wrong*.

Finally, exploiting the readings of the encoders, we can define the last measurement transformation

$$\begin{aligned} \eta_1 &= \rho_1 \\ \eta_2(k, j) &= \rho_1 + \rho_2 - w_4(k, j) \\ \eta_3(k, j) &= w_4(k, j) - \rho_1 \\ \eta_4(k, j) &= w_2(k) + w_4(k, j) - \rho_1 - \rho_2. \end{aligned} \tag{7.21}$$

The transformation method is represented in Fig. 7.3a. From (7.21) one can notice that for the pair (k^*, j^*) defined before, we obtain a direct measure of the generalized coordinates, i.e. $\boldsymbol{\eta}(k^*, j^*) = [\eta_1\ \ \eta_2(k^*, j^*)\ \ \eta_3(k^*, j^*)\ \ \eta_4(k^*, j^*)]^\top = [\boldsymbol{\eta}_1^\top(k^*, j^*)\ \ \boldsymbol{\eta}_2^\top(k^*, j^*)]^\top = [\varphi_1\ \ \varphi_2\ \ \theta_1\ \ \theta_2]^\top$. While, for the pairs $(k, j) \neq (k^*, j^*)$, $\boldsymbol{\eta}(k, j)$ is a wrong measurement of the configuration. From a single set of measures it is not possible to discriminate which is the correct pair (k^*, j^*) corresponding to the correct $\boldsymbol{\eta}$, nevertheless, in Sect. 7.4.4 we show a discriminating method exploiting the dynamics, similar to the one proposed in Sect. 4.8.

For the purpose of proving the observability of the system and for designing the observer we consider $\boldsymbol{\eta} = \boldsymbol{\eta}(k^*, j^*)$.

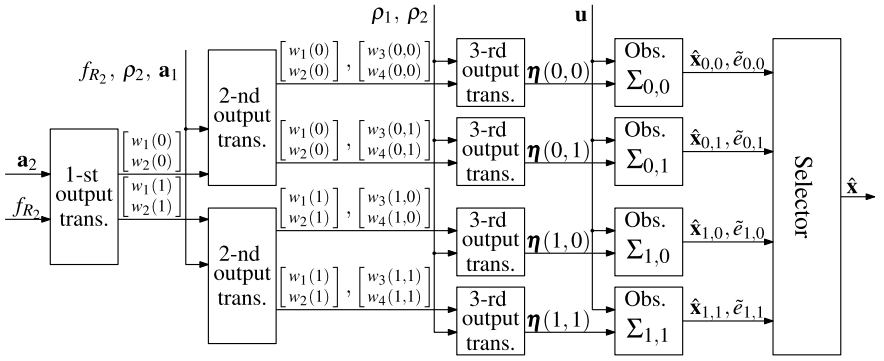

(a) Global Observer.

(b) Observer $\Sigma_{k,j}$.

Fig. 7.3 Graphic representation of the observer. © 2020 IEEE. Reprinted, with permission, from [1]

7.4.2 Observability

In order to study the observability of the system and to design an observer of the state, we first rewrite the system in a state space form. We can rewrite (7.6) and the measurements function (7.21) as:

$$\dot{\mathbf{x}} = \mathbf{A}\mathbf{x} + \mathbf{B}\begin{bmatrix} \boldsymbol{\Sigma}(\mathbf{x}, \mathbf{u}_1) \\ J^{-1}\mathbf{u}_2 \end{bmatrix} \tag{7.22a}$$

$$\boldsymbol{\eta} = \mathbf{C}\mathbf{x}, \tag{7.22b}$$

where $\mathbf{A} = \text{diag}(\mathbf{A}_1, \mathbf{A}_2, \mathbf{A}_3, \mathbf{A}_4)$, $\mathbf{B} = \text{diag}(\mathbf{B}_1, \mathbf{B}_2, \mathbf{B}_3, \mathbf{B}_4)$, $\mathbf{C} = \text{diag}(\mathbf{C}_1, \mathbf{C}_2, \mathbf{C}_3, \mathbf{C}_4)$ and

$$\mathbf{A}_i = \begin{bmatrix} 0 & 1 \\ 0 & 0 \end{bmatrix}, \quad \mathbf{B}_i = \begin{bmatrix} 0 \\ 1 \end{bmatrix}, \quad \mathbf{C}_i = \begin{bmatrix} 1 & 0 \end{bmatrix} \quad \forall i = 1, \ldots, 4$$

$$\boldsymbol{\Sigma}(\mathbf{x}, \mathbf{u}_1) = -\boldsymbol{M}(\mathbf{x})^{-1}\boldsymbol{c}(\mathbf{x}) + \boldsymbol{M}(\mathbf{x})^{-1}\bar{\mathbf{Q}}_{\boldsymbol{\varphi}}(\mathbf{x})\boldsymbol{u}_1. \tag{7.23}$$

Notice that $\boldsymbol{M}(\mathbf{x})$ is always invertible. Writing (7.22) as $\dot{\mathbf{x}} = \mathbf{f}(\mathbf{x}, \mathbf{u})$, and $\boldsymbol{\eta} = \mathbf{h}(\mathbf{x})$. the system results observable if the nonlinear observability matrix $O(\mathbf{x}, \mathbf{u}) =$

$\left[\frac{\partial \mathbf{h}(\mathbf{x})}{\partial \mathbf{x}}, \frac{\partial \dot{\mathbf{h}}(\mathbf{x})}{\partial \mathbf{x}}, \ldots, \frac{\partial \mathbf{h}^{(7)}(\mathbf{x})}{\partial \mathbf{x}}\right]^\top \in \mathbb{R}^{4\cdot 8\times 8}$ is full rank [3]. We can notice that

$$O(\mathbf{x},\mathbf{u})_1 = \left[\frac{\partial \mathbf{h}(\mathbf{x})}{\partial \mathbf{x}}, \frac{\partial \dot{\mathbf{h}}(\mathbf{x})}{\partial \mathbf{x}}\right]^\top = \left[\mathbf{C}^\top \ (\mathbf{C}A)^\top\right]^\top.$$

Changing the order of the rows we obtain $O(\mathbf{x},\mathbf{u})'_1 = \mathbf{I}_8$, that is full rank for every $\mathbf{x} \in \mathbb{R}^8$ and $\mathbf{u} \in \mathbb{R}^4$. This implies that also $O(\mathbf{x},\mathbf{u})$ is always full rank, i.e.,

Proposition *Consider the system described by (7.6) with two on-board accelerometers, mounted on each vehicles, and two encoders. One is attached to the ground and connected to the first link, and one is mounted on the first vehicle and connected to the second link. Then, the system is observable except for the zero internal force cases, i.e., $f_{L1} = 0$ or $f_{L2} = 0$.* □

Although we proved Proposition 7.4.2 only for the fourth case of Table 7.1, actually, the result shows a more general sufficient observability condition. Indeed, independently from the available sensors, whenever there are some output transformations that translate the original measurements into direct measures of $\mathbf{q}$, then the system is observable, i.e.,

Proposition *Consider the system described by (7.22a) and a set of measurements $\mathbf{w} = \mathbf{h}(\mathbf{x},\mathbf{u}) \in \mathbb{R}^p$, where $p \in \mathbb{R}_{\geq 1}$. Define $\mathcal{X}$ the state space and $\mathcal{U}$ the control inputs space. If there exists a subspace $\mathcal{D} \subseteq \mathcal{X} \times \mathcal{U}$ and a measurement transformation function $\boldsymbol{\Gamma} : \mathbb{R}^p \to \mathbb{R}^4$ valid in $\mathcal{D}$, such that $[\varphi_1 \ \varphi_2 \ \theta_1 \ \theta_2]^\top = \boldsymbol{\Gamma}(\mathbf{w})$, then the system is observable for every $\mathbf{x}$ and $\mathbf{u}$ in $\mathcal{D}$, and can be written in the form of (7.22).* □

7.4.3 High Gain Observer

For the sets of measurements that fulfill the condition of Proposition 7.4.2, and in particular for the case 4 of Table 7.1 we show in this section the design of an observer based on HGO (see Sect. 2.4).

Considering the system (7.22) we define $\boldsymbol{\zeta} = [\boldsymbol{\zeta}_1^\top \ \boldsymbol{\zeta}_2^\top]^\top = [\zeta_1 \ \zeta_2 \ \zeta_3 \ \zeta_4]^\top = [x_1 \ x_2 \ x_3 \ x_4]^\top$ and $\mathbf{z} = [\mathbf{z}_1^\top \ \mathbf{z}_2^\top]^\top = [z_1 \ z_2 \ z_3 \ z_4]^\top = [x_5 \ x_6 \ x_7 \ x_8]^\top$. The system (7.22) can be then written as

$$\begin{cases} \dot{\boldsymbol{\zeta}} = \mathbf{A}_{\boldsymbol{\zeta}}\boldsymbol{\zeta} + \mathbf{B}_{\boldsymbol{\zeta}}\boldsymbol{\Sigma}(\boldsymbol{\zeta}, \boldsymbol{\eta}_2, \mathbf{u}_1) \\ \boldsymbol{\eta}_1 = \mathbf{C}_{\boldsymbol{\zeta}}\boldsymbol{\zeta} \end{cases} \qquad \begin{cases} \dot{\mathbf{z}} = \mathbf{A}_{\mathbf{z}}\mathbf{z} + \mathbf{B}_{\mathbf{z}}\mathbf{u}_2 \\ \boldsymbol{\eta}_2 = \mathbf{C}_{\mathbf{z}}\mathbf{z}, \end{cases} \tag{7.24}$$

where $\mathbf{A}_{\boldsymbol{\zeta}} = \text{diag}(\mathbf{A}_1, \mathbf{A}_2)$, $\mathbf{B}_{\boldsymbol{\zeta}} = \text{diag}(\mathbf{B}_1, \mathbf{B}_2)$, $\mathbf{C}_{\boldsymbol{\zeta}} = \text{diag}(\mathbf{C}_1, \mathbf{C}_2)$, $\mathbf{A}_{\mathbf{z}} = \text{diag}(\mathbf{A}_3, \mathbf{A}_4)$, $\mathbf{B}_{\mathbf{z}} = \text{diag}(\mathbf{B}_3, \mathbf{B}_4)J^{-1}$, $\mathbf{C}_{\mathbf{z}} = \text{diag}(\mathbf{C}_3, \mathbf{C}_4)$. Having replaced θ_1 and θ_2 with their measures $\boldsymbol{\eta}_2$ in the dynamics of $\boldsymbol{\zeta}$, the two systems become completely independent, moreover, the second one is linear, therefore we can design for it a classical Luenberger observer

$$\dot{\hat{\mathbf{z}}} = \mathbf{A}_{\mathbf{z}}\hat{\mathbf{z}} + \mathbf{B}_{\mathbf{z}}\mathbf{u}_2 + \mathbf{H}_{\mathbf{z}}(\boldsymbol{\eta}_2 - \mathbf{C}_{\mathbf{z}}\hat{\mathbf{z}}), \tag{7.25}$$

where $\mathbf{H}_{\mathbf{z}} = \text{diag}(\mathbf{H}_{\mathbf{z}_1}, \mathbf{H}_{\mathbf{z}_1})$ and $\mathbf{H}_{\mathbf{z}_i} = [\beta_1^i \;\; \beta_2^i]^\top$, whose elements, $\beta_j^i \in \mathbb{R}_{>0}$ can be set to place the poles of the error dynamics, $\boldsymbol{e}_{\mathbf{z}_i} = \mathbf{z}_i - \hat{\mathbf{z}}_i$. Instead, for the first system, thanks to its particular triangular form, it is possible to use the following HGO

$$\dot{\hat{\boldsymbol{\zeta}}} = \mathbf{A}_{\boldsymbol{\zeta}}\hat{\boldsymbol{\zeta}} + \mathbf{B}_{\boldsymbol{\zeta}}\boldsymbol{\Sigma}(\hat{\boldsymbol{\zeta}}, \boldsymbol{\eta}_2, \mathbf{u}_1) + \mathbf{H}_{\boldsymbol{\zeta}}(\boldsymbol{\eta}_1 - \mathbf{C}_{\boldsymbol{\zeta}}\hat{\boldsymbol{\zeta}}), \tag{7.26}$$

where $\mathbf{H}_{\boldsymbol{\zeta}} = \text{diag}(\mathbf{H}_{\boldsymbol{\zeta}_1}, \mathbf{H}_{\boldsymbol{\zeta}_1})$ and $\mathbf{H}_{\boldsymbol{\zeta}_i} = [\frac{\alpha_1^i}{\epsilon} \;\; \frac{\alpha_2^i}{\epsilon^2}]^\top$, with $\epsilon \in \mathbb{R}_{>0}$, and the gains $\alpha_j^i \in \mathbb{R}_{>0}$ are set such that the roots of $s^2 + \alpha_1^i s + \alpha_2^i$ have negative real part. The gains (α_1^i, α_2^i) influence the convergence rate of the estimation of the ith elevation angle and its derivative, i.e., φ_i and $\dot{\varphi}_i$. A schematic representation of the observer is given in Fig. 7.3b.

7.4.4 *Disambiguation of $\boldsymbol{\eta}$*

The output transformations described in Sect. 7.4.1 generates four different set of measurements, $\boldsymbol{\eta}(k, j)$ with $k, j \in \{0, 1\}$, of which only one is correct.

As represented in Fig. 7.3a, for each $k, j \in \{0, 1\}$, we implement an observer of the state, Σ_{kj}, using (7.25) and (7.26), based on the measurements $\boldsymbol{\eta}(k, j)$. Therefore we obtain four estimates of the state, one for each measurement pair, $\hat{\mathbf{x}}_{0,0}$, $\hat{\mathbf{x}}_{0,1}$, $\hat{\mathbf{x}}_{1,0}$, $\hat{\mathbf{x}}_{1,1}$, and the correct one has to be recognized.

Define $\hat{\mathbf{w}} = [\hat{\mathbf{a}}_1^\top \;\; \hat{\mathbf{a}}_2^\top \;\; \hat{\rho}_1 \;\; \hat{\rho}_2]^\top$ as the vector that contains the measurements computed with the estimated state, i.e.,

$$\hat{\rho}_1 = \hat{x}_1, \quad \hat{\rho}_2 = \hat{x}_3 + \hat{x}_5, \quad \hat{\mathbf{a}}_i = \hat{R}_W^{B_i}(\hat{\mathbf{p}}_{B_i} - g\boldsymbol{z}_W),$$

where $\hat{R}_W^{B_i} = R_W^{B_i}(\hat{\mathbf{x}})$, and $\hat{\mathbf{p}}_{B_i}$ is calculated considering the system model (i.e., no numerical differentiation is needed)

$$\begin{aligned}
\hat{\mathbf{p}}_{B_1} &= -l_1\mathbf{d}_1(\hat{x}_1)\hat{x}_2^2 + l_1\mathbf{d}_1^\perp(\hat{x}_1)\hat{x}_2 \\
\hat{\mathbf{p}}_{B_2} &= \hat{\mathbf{p}}_{B_1} - l_2\mathbf{d}_2(\hat{x}_3)\hat{x}_4^2 + l_2\mathbf{d}_2^\perp(\hat{x}_3)\hat{x}_4.
\end{aligned}$$

In the previous equations $\hat{x}_2$ and $\hat{x}_4$ are the estimation of the angular acceleration of the elevations calculated replacing the estimated state into (7.23), i.e., $[\hat{x}_2 \;\; \hat{x}_4]^\top = \boldsymbol{\Sigma}(\hat{\mathbf{x}}, \mathbf{u}_1)$ (no numerical differentiation needed in this case either).

In order to choose the correct estimation among the four, we propose a method based on the minimal prediction error, similar to the one used in Sect. 4.8. For each observer we compute a prediction error $\tilde{e}_{k,j}$ smoothed with an exponential discount factor:

$$\dot{\tilde{e}}_{k,j} = \lambda(\|\mathbf{w} - \hat{\mathbf{w}}_{k,j}\| - \tilde{e}_{k,j}),$$

where $\lambda \in \mathbb{R}_{>0}$ sets the discount rate and $\mathbf{w} = [\mathbf{a}_1^\top \ \mathbf{a}_2^\top \ \rho_1 \ \rho_2]^\top$. Then, the estimation of the observer with minimum prediction error is chosen, i.e., $\hat{\mathbf{x}} = \hat{\mathbf{x}}_{k^*,j^*}$ s.t. $\{k^*, j^*\} = \arg\min_{\mathrm{k,j}\in\{0,1\}}(\tilde{e}_{k,j})$. Figure 7.3 shows the estimator structure.

7.4.5 Discussion on the Proposed Method

7.4.5.1 Zero Internal Force Case

As we previously noticed, if one of the link internal forces is zero then w_2 or w_4 cannot be determined. We noticed an analogous singularity in Sects. 4.7 and 4.8 for the single tethered system as well. Nevertheless, we showed that if the desired internal force is passing through zero for a sufficiently short (ideally zero) time interval, one can still use the proposed observes in practice by updating the filter without the correction term in that time instants. For the multi-tethered system this implies to impose

$$\begin{aligned} \dot{\hat{\mathbf{z}}} &= \mathbf{A}_\mathbf{z}\hat{\mathbf{z}} + \mathbf{B}_\mathbf{z}\mathbf{u}_2 \\ \dot{\hat{\boldsymbol{\zeta}}} &= \mathbf{A}_\zeta\hat{\boldsymbol{\zeta}} + \mathbf{B}_\zeta\boldsymbol{\Sigma}(\hat{\boldsymbol{\zeta}}, \hat{\mathbf{z}}, \mathbf{u}_1) \end{aligned} \qquad \text{if } w_1 = 0 \text{ or } w_3 = 0.$$

During this instant the observation is done in 'open loop' only using the model dynamics, thus the error dynamics becomes non strictly stable for a short moment. However, the dynamics returns asymptotically stable as soon as the internal force becomes non-zero again, as it is shown in Sect. 7.5 by simulations.

7.4.5.2 Applicability

The transformation method showed for the case 4 in Table 7.1 can be applied also to other sets of sensors. Last column of Table 7.1 specifies for which cases the method is able to transform the original measurements into direct measures of the system configuration. For cases 1 and 2, the measurements transformations are very similar to those derived for case 4. For the remaining cases it is not possible to apply the proposed method. In particular for the cases 3, 5, 7 we cannot compute the transformation (7.20). While, for the case 6, the problem lies in the last transformation (7.21).

7.4.5.3 Loop Stability

For the control law described in Sect. 7.3, the knowledge of the state is sufficient in order to close the loop. Thus we can use as feedback the state estimation provided by the proposed observer. Then a similar reasoning to the one in Sects. 4.7 and 4.8

can be done to prove that there exist a ϵ^* such that, for every $0 < \epsilon \leq \epsilon^*$ in (7.26), the closed loop system with the observer is exponentially stable, except for the zero thrust and zero internal force cases.

7.5 Numerical Validation

We tested the closed loop system (observer + controller) in simulation using two aerial robots with $m_{Ri} = 1\,\text{kg}$ and $J_{Ri} = 0.15\,\text{kg m}^2$, and two links with $l_i = 2\,\text{m}$ ($i = 1, 2$). In order to obtain a reasonable fast tracking of the desired trajectories we set the gains such as the error dynamics relative to φ_1, φ_2 and f_{L1}, f_{L2} has poles in $(-3, -6, -9, -12)$ and $(-5, -10)$, respectively.

Regarding the convergence of the state estimation, we set $\epsilon = 0.1$ and the gains (α_1^i, α_2^i) such as the roots of $s^2 + \alpha_1^i s + \alpha_2^i$ are $(-2, -3)$. We set $\mathbf{H}_{\mathbf{z}_i}$ such that the error dynamics of the estimation of θ_1 and θ_2 has poles in $(-15, -25)$. Finally, the discount rate of the prediction error dynamics is set to $\lambda = 20$. These gains values, replicated identically for each of the four observers, guarantee the stability of the closed-loop system.

To show the ability of the proposed observer to exponentially converge to the real state, we initialize it with an error of 5° relatively to the elevation and pitch angles. We propose two different simulations:

(i) the first, whose results are plotted in Fig. 7.4, shows the performances of the global closed loop system in the particular case of inversion of the internal force. In particular, the trajectory of the end-effector is a trajectory of class C^3 from the initial position $\mathbf{p}_{B_2}(0) = [2.5\ \ 0\ \ 2]^T$ to the final $\mathbf{p}_{B_2}(t_f) = [-0.7\ \ 0\ \ 0.7]^T$. While the desired internal force along the links is a trajectory of class C^1 from the initial tension of 10 N to the final compression of −10 N.

(ii) In the second simulation, reported in Fig. 7.5, we replicate a plausible real scenario where the system is controlled as a two-link robot. The desired trajectory of the end-effector is planned in the Cartesian space as a sequence of three arcs of ellipse in order to enter, stop on each room of a plausible building, and then return to the initial position. By inverse kinematics the desired trajectories of the two elevations are derived. In the meanwhile a constant tension of 5 N is required on the two links for the hole duration of the task.

To better represent the behavior of the system, Figs. 7.4c and 7.5c show the stroboscopic evolution of the system where the flow of time is provided by the change of color. To graphically represent the internal force variation, the link is drawn as a dashed line with a thinner width when the tension is higher, and as a solid line with a wider width when the compression is higher.

From Figs. 7.4 and 7.5 one can notice that the estimation of the state converges to the real one in less than one second, in any dynamic condition. Moreover, for the first simulation, the prediction error does not increase even when the desired internal force passes through zero. Although during the transient of the estimation the controller

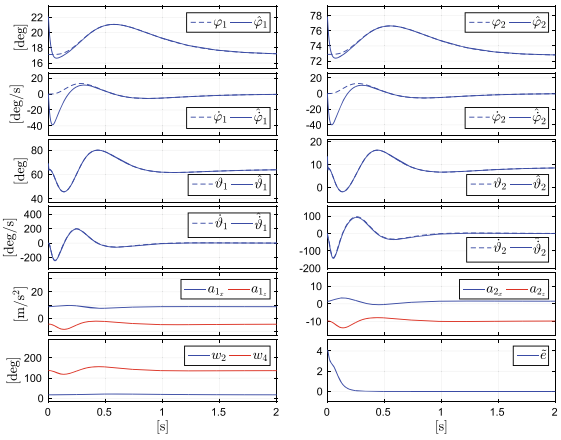

(a) Observer Results: the plot shows only the first 2 seconds of simulation. After this time the estimation follows the state with high fidelity thus the rest of the simulation is not displayed.

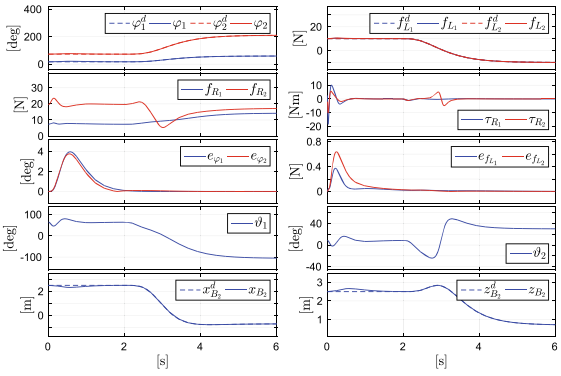

(b) Controller Results.

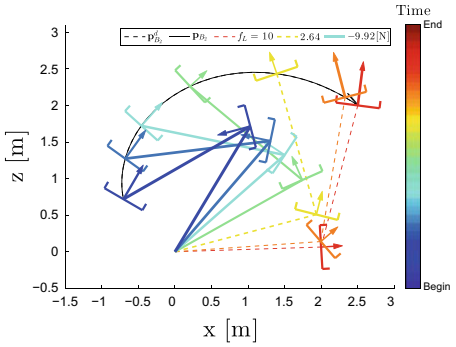

(c) Trajectory visualization from time Begin = 0 [s] to End = 6 [s]. The thrust arrow is drawn thicker and longer when the thrust intensity is higher.

Fig. 7.4 Simulation results: point to point motion. © 2020 IEEE. Reprinted, with permission, from [1]

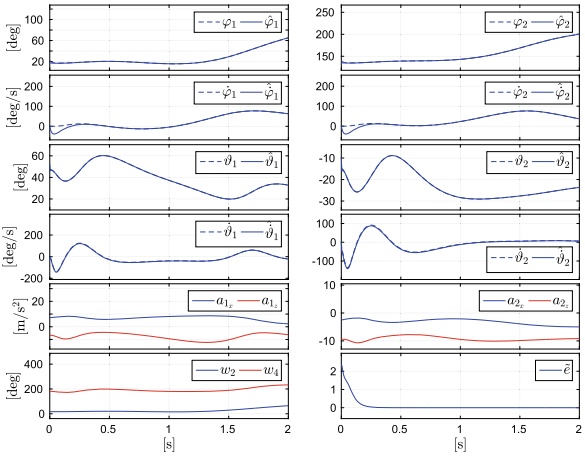

(a) Observer Results: the plot shows only the first 2 seconds of simulation.

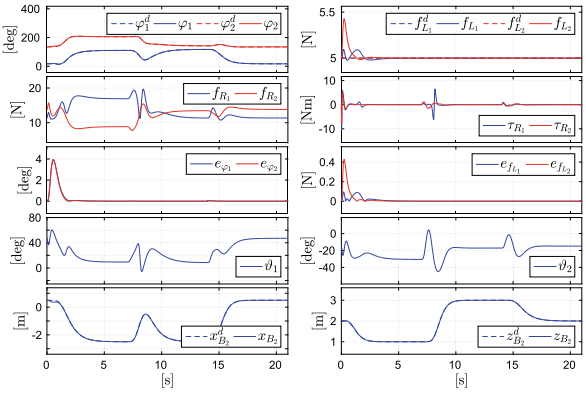

(b) Controller Results.

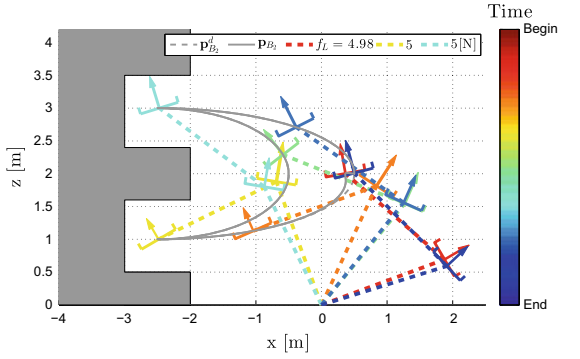

(c) Trajectory visualization from time Begin = 0 [s] to End = 21 [s].

Fig. 7.5 Simulation results: example of a search and rescue task. © 2020 IEEE. Reprinted, with permission, from [1]

shows a non zero tracking error, actually, as soon as the estimation error goes to zero, the outputs follow the desired trajectory with high fidelity during the remaining time of the simulation. An animation of the simulations is also available at [4].

References

1. Tognon, M., Franchi, A.: Nonlinear observer for the control of bi-tethered multi aerial robots. In: 2015 IEEE/RSJ International Conference on Intelligent Robots and Systems, pp. 1852–1857, Hamburg, Germany (2015)
2. Tognon, M., Franchi, A.: Control of motion and internal stresses for a chain of two underactuated aerial robots. In: 14th European Control Conference, pp. 1620–1625, Linz, Austria (2015)
3. Marino, R., Tomei, P.: Nonlinear Control Design: Geometric. Prentice Hall, Adaptive and Robust (1996)
4. video 4: Nonlinear observer for the control of bi-tethered multi aerial robots. https://www.youtube.com/watch?v=JdMAEneWolk (2015)